This document is the accepted manuscript version of the following article:
Mussetti, G., Brunner, D., Allegrini, J., Wicki, A., Schubert, S., & Carmeliet, J. (2019). Simulating urban climate at sub‐kilometre scale for representing the intra‐urban variability of Zurich, Switzerland. International Journal of Climatology, (19 pp.). https://doi.org/10.1002/joc.6221

# High-resolution simulation of urban climate at local scale during a heat wave in Zurich

Gianluca Mussetti[1,2,3*], Dominik Brunner[1], Jonas Allegrini[2,3], Sebastian Schubert[4], Jan Carmeliet[2,3]

1 – Laboratory of Air Pollution / Environmental Technology, Empa, 8600 Dübendorf, Switzerland;

2 – Laboratory of Multiscale Studies in Building Physics, Empa, 8600 Dübendorf, Switzerland;

3 – Chair of Building Physics, ETH Zürich, 8093 Zürich, Switzerland;

4 - Geography Department, Humboldt-Universität zu Berlin, 10099 Berlin, Germany.

**Short title:** HIGH-RESOLUTION URBAN CLIMATE SIMULATION

*** corresponding author:**

Email: gianluca.mussetti@empa.ch
Tel: +41 58 765 60 91
Address: Empa, Üeberlandstrasse 129, 8600 Dübendorf, Switzerland

**Email addresses:**

gianluca.mussetti@empa.ch (G. Mussetti), dominik.brunner@empa.ch (D. Brunner), jonas.allegrini@empa.ch (J. Allegrini), sebastian.schubert@geo.hu-berlin.de (S. Schubert), cajan@ethz.ch (J. Carmeliet)

**Keywords:**

Urban climate; local scale; neighbourhood scale; high resolution; heat wave; intra-urban variability

## Abstract

In the face of an increasing number of urban climate modelling studies performed at sub-kilometre resolution, systematic investigations of the performance of high-resolution urban climate simulations and their dependency on spatial resolution are still very sparse. This study investigates the impact of the scale of representation of the urban area on the urban climate

simulation with a multi-layer urban canopy model integrated in a mesoscale numerical weather prediction model for different sub-kilometre resolutions. The potential of using such a model system for representing the intra-urban climate variability is explored. The weather and climate model CCLM, coupled with the multi-layer urban canopy model DCEP (CCLM-DCEP), was used at increasing resolution from 1 km to 250 m grid spacing to simulate the pronounced heat wave event of June-July 2015 over the city of Zurich, Switzerland. CCLM-DCEP improved the model performance during night-time in comparison to the standard CCLM, especially at open midrise sites. Small-scale features such as urban parks and large railway areas started to be resolved at sub-kilometre grid spacing, producing a spatial variability in air temperature of up to 2 °C and wind speed of up to 1.5 m $s^{-1}$ within a radius of 1 km inside the city. Due to the sparsity of meteorological observations available in the city, a thorough evaluation of the model performance at the different resolutions was not feasible. However, an improvement in simulated air temperature and wind speed with model resolution was noticeable at compact midrise sites. CCLM-DCEP showed the potential to represent the urban climate at the neighbourhood scale when used at high (sub-kilometre) resolution, which is needed to support applications such as urban planning, building energy use and urban air quality.

## 1. Introduction

Cities are known to impact the weather and climate both locally and regionally, producing a characteristic *urban climate*. The best known *urban climate* effect is the air temperature increase in urban areas compared to their rural surroundings – the so-called *Urban Heat Island* (UHI) effect. Numerous urban climate studies have been performed over the last 100 years (Arnfield, 2003), with a focus today on its implications for energy use, human comfort, air pollution, and urban ecology (Roth, 2011).

Traditionally, the multiple scales and physical processes found in the urban area have been parametrised using simplifying assumptions, leading to *urban canopy models* UCMs (or *urban*

*land surface models*). UCMs simulate the exchange of energy and momentum between urban surfaces and the atmosphere and have been coupled with weather and climate models ranging from the mesoscale ($10^4$-$10^5$ m) to the global scale (e.g. Masson, 2006; Oleson *et al.*, 2008). While UCMs are typically designed to represent processes at the local scale ($10^1$ - $10^3$ m), weather and climate models have been traditionally limited to the mesoscale.

Only very recently, the increase in computational power and new physical parameterisations have led to the usage of these models at resolutions down to the kilometre or even sub-kilometre scale (e.g. Grawe *et al.*, 2013; Leutwyler *et al.*, 2016; Li *et al.*, 2013; Sharma *et al.*, 2017). These advances offer now the opportunity to exploit UCMs at the local scale and therefore to model the intra-urban climate variability. Urban simulation at local scale has the potential to better support applications such as urban planning, building energy use and urban air quality.

In the face of several urban climate studies performed at sub-kilometre resolution (Flagg and Taylor, 2011; Li *et al.*, 2013; Miao *et al.*, 2009; Ronda *et al.*, 2017), systematic investigations of the performance of high-resolution urban climate simulations and their dependency on model spatial resolution are still very sparse. Flagg and Taylor (2011) investigated the sensitivity of the surface energy balance, canopy layer and boundary layer meteorology to the resolution at which the urban surface is represented. They found a significant dependency on model resolution of latent heat fluxes from the natural surface and sensible heat fluxes from the urban canopy. They also showed, for a coastal city, that the timing of the passage of the lake-breeze front depended on the resolution of the simulation. Ronda *et al.* (2017) investigated the performance of an improved version of the Weather Research and Forecasting model (WRF) over an urban area at different model resolutions. Using a single layer urban canopy model, they found improved performance at high resolution, but they did not identify which components were responsible. Loridan *et al.* (2013) assessed the performance of a new on-line UCM in representing the intra-urban variability of energy fluxes. They found greater energy storage and less evaporation in the

dense city centre compared to the residential surroundings. However, they did not quantify the response of the model to different grid spacing. Li and Bou-Zeid (2014) performed a sensitivity study on the impact of different physical parameterisations (PBL and surface-layer scheme) without investigating the sensitivity to the model resolution. All the previous studies used a single-layer UCM which makes their results not easily transferable to multi-layer UCMs, where the urban canopy is divided into several layers in the vertical direction. Multi-layer UCMs, like the one used in this study, have the advantage of being able to better integrate high-resolution information because of their greater flexibility and more explicit representation of different urban morphologies. Depending on their design, UCMs may be sensitive to model resolution due to nonlinear effects and potential scale-dependencies of the parameterisations, a known issue in land surface modelling (Giorgi and Avissar, 1997). Comparing the performance at different model resolutions is, therefore, an essential step to characterise any scale-dependence of a UCM. This brief review shows that there is still a need for further investigating the impact of model resolution on the accuracy of urban climate modelling, as also suggested by Martilli (2007) and Chen *et al.* (2012).

This study aims to evaluate the impact of the scale of representation of the urban area on the urban climate simulation with a multi-layer UCM integrated in a mesoscale weather prediction model for different sub-kilometre model resolutions. Moreover, we investigated the potential of using such a model system for representing the intra-urban climate variability. The medium-sized city of Zurich, Switzerland has been selected for this study as it reflects the common characteristics of many European cities: complex urban morphology with strong heterogeneity in local urban climates (Stewart and Oke, 2012).

## 2. Methods and data

### 2.1 Study area & model setup

The city of Zurich is located in north-central Switzerland at the north-western tip of Lake Zurich (Figure 1 a). Situated at the border between oceanic climate (Köppen climate classification Cfb) and humid continental climate (Köppen climate classification Dfb), Zürich experiences four distinct seasons and temperatures. The lowest monthly mean of daily minimum temperature is observed in January with −2 °C and the highest monthly mean of daily maximum temperature in July with 24 °C. There are on average 30 so-called summer days (maximum temperature equal to or above 25 °C) and 5.8 so-called heat days (maximum temperature equal to or above 30 °C) per year (MeteoSwiss, 2017).

A heat wave swept across central Europe in summer 2015 (Ionita *et al.*, 2017). The seasonal mean (June–August) surface air temperature was 2.4 °C above the 1964 – 1993 mean (Buwen *et al.*, 2016). The period of 22 June – 10 July 2015 (18 days) featured a steady temperature rise from 23 June to 7 July followed by a dramatic drop in temperature by more than 15°C due to the passage of a cold front on 8 July (Figure 2 a). The air temperatures in the urban compact midrise site were substantially higher than in the rural site, especially at night. The UHI intensity, defined as the air temperature difference between the urban and the rural area, reached values up to 5°C (Figure 2 b).

We performed the simulations with the non-hydrostatic limited-area weather prediction and climate model COSMO in Climate Mode (CCLM), version 5. CCLM evolved from the operational weather forecast Local Model (LM) of the German Weather Service (Steppeler *et al.*, 2003) and it is being developed by a consortium of weather services in Europe and by the CLM-Community for climate applications (Rockel *et al.*, 2008). The planetary boundary-layer scheme is based on Mellor and Yamada (1982). The radiation scheme is based on the δ-two-stream version of the radiative transfer equation (Ritter and Geleyn, 1992) and shallow convection is parametrized by

the Tiedkte (1989) scheme. Details for the multi-layer soil model, vegetation parametrisation and the cloud microphysics scheme are given in Doms *et al.* (2011). CCLM has been used previously for urban climate applications by e.g. Trusilova *et al.* (2015), Wouters *et al.* (2016) and Grossman-Clarke *et al.* (2017).

We applied CCLM over a domain (Figure 1 a) of the size of approx. 50 km x 50 km with decreasing horizontal grid spacing of 1 km, 500 m and 250 m. 76 levels were used in the vertical direction, with 6 and 23 levels in the first 100 m and 1000 m, respectively. Atmospheric analyses from the operational COSMO-2 model, operated by the Federal Office of Meteorology and Climatology of Switzerland (MeteoSwiss), were used as initial and boundary conditions for all simulations. The analyses cover the entire Alpine range with a resolution of about 2 km. The analyses are generated from the operational forecast using a nudging technique (Schraff, 1997) applied to near-surface and vertical profile observations of pressure, relative humidity and wind. As external input parameters for CCLM, the 1'' global digital elevation map ASTER (https://asterweb.jpl.nasa.gov) for topography, the 10'' land use dataset GlobCover 2009 (Loveland *et al.*, 2000) for land cover and the 30'' Harmonized World Soil Database (FAO *et al.*, 2009) (Fischer *et al.*, 2008) for soil characteristics were used in this study. The datasets had been pre-processed through the PrEProcessor of time-invariant parameters tool (Smiatek *et al.*, 2008). A summary of the simulations and input data is given in Table 1.

## 2.2 Urban parameterization

Two parameterisations of different complexity were used to represent the urban area in the CCLM simulation: the standard bulk parameterisation (STD) of CCLM and the Double-Canyon Effect Parameterization (DCEP, Schubert *et al.*, 2012). CCLM used with STD and DCEP is called hereinafter CCLM-STD and CCLM-DCEP, respectively.

In the standard parameterisation STD, urban areas are modelled using a bulk-transfer scheme with a fixed fraction (0.9) of impervious surfaces with an increased surface roughness length ($z_0 = 1.0\,m$), reduced vegetation cover ($0.1$) and leaf area index ($LAI = 1$). These assumptions are applied uniformly over the entire urban area. The advantage of this approach is the low demand on input parameters and the possibility to represent the urban surface within the standard land surface scheme TERRA of CCLM (Doms *et al.*, 2011). However, this type of simple parametrization is likely not able to fully represent the characteristics of urban areas that influence the atmosphere.

DCEP is a multi-layer urban canopy model based on the Building Effect Parameterization (BEP; Martilli *et al.*, 2002). Urban areas are represented as a statistical ensemble of two-dimensional street canyons characterised by specific orientation, building and street width, and building height distribution. Radiation exchange for both long- and shortwave radiation between roof, wall and street surfaces is simulated. As an extension of the original BEP scheme, DCEP adds the radiation exchange between roof and wall surfaces in the street canyon for better representing urban regions with large variety of building heights (Schubert *et al.*, 2012). DCEP calculates energy and momentum fluxes from street, wall and roof surfaces to the lowest layers of the atmospheric model. The vertical resolution of DCEP is enhanced compared to the atmospheric model resolution and can be specified independently, allowing a detailed representation of the urban canyon without affecting the atmospheric model resolution. The surface energy and momentum flux from natural and urban surfaces of an atmospheric model grid cell are averaged using the corresponding areal fractions, e.g. for the sensible heat flux:

$$SHF_{tot} = f_{urb} \times SHF_{urb} + f_{nat} \times SHF_{nat}\,, \tag{1}$$

where $SHF_{tot}$ is the total sensible heat flux [W m$^{-2}$], $f_{urb}$ is the urban fraction [-], $SHF_{urb}$ is the sensible heat flux from urban surfaces [W m$^{-2}$], $f_{nat}$ is the natural fraction [-] with $f_{urb} = 1 -$

$f_{nat}$, $SHF_{nat}$ is the sensible heat flux from natural surfaces [W m$^{-2}$]. Further details of the coupling between DCEP and the atmospheric model are provided in Schubert *et al.* (2012).

DCEP requires additional input data such as distribution of building height and orientation, roof and road width and the fraction of non-natural surface. Detailed information on the additional input data is given in Section 2.3. The material properties of roof (R), wall (W) and street surfaces (G) follow the proposals of Martilli *et al.* (2002): the corresponding emissivities are $\varepsilon_R = \varepsilon_W = 0.9$ , $\varepsilon_G = 0.95$ and the thermal diffusivities are $k_R = k_W = 0.67 \times 10^{-6}\, m^2\, s^{-1}$ , $k_G = 0.29 \times 10^{-6}\, m^2\, s^{-1}$. Furthermore, the same value of the volumetric specific heat capacity is used for all surfaces, $c_R = c_W = c_G = 2.3 \times 10^6\, J\, m^{-3}\, K^{-1}$. Typical albedo values for roof and street surfaces are chosen according to Loridan and Grimmond (2012): $\alpha_R = 0.15$ and $\alpha_G = \alpha_W = 0.1$. DCEP is applied here only for grid cells with a building fraction $f_{build} > 0.1$, where $f_{build}$ is the fraction of the grid cell surface covered by buildings.

## 2.3 Observations and input data

We compared the results of the CCLM simulation with measurements from six surface stations located in the urban area (see Figure 1 b). The sites have been classified according to the Local Climate Zone (LCZ) definitions by Stewart & Oke (2012) and grouped accordingly to allow interpreting the results in terms of the local environment of the sites. The sites classification was supported by personal surveys and aerial images. The sites of KAS (Zürich-Kaserne) and SCH (Zürich-Schimmelstrasse) are situated in the densely built-up core of Zurich, classified here as compact midrise (LCZ 2). A dense mix of midrise buildings (3–9 stories) is present in this area, with mostly paved land cover and few or no trees. Construction materials are mainly concrete, brick and stone. The sites of ROS, STA and SMA are situated in the immediate surroundings of the city core of Zurich, classified as open midrise (LCZ 5). A more open arrangement of midrise buildings (3-9 stories) is present here, with abundance of pervious land covers such as small parks and trees. Construction materials are mainly concrete, brick and stone. The site of REH is

202 classified as Rural - low plants (LCZ D). Featureless landscape of grass is present, with the closest
203 building located at 100 m distance.

204 Air temperatures are measured at approx. 2 m height at all the sites. Instruments are ventilated
205 and shielded as recommended by WMO (2008). The surface underneath the temperature sen-
206 sors is typical of the corresponding LCZ, i.e. artificial for urban and natural for rural sites, respec-
207 tively.

208 Wind speeds are measured at varying heights at the different sites, but always above the *urban*
209 *canopy layer* and following the recommendations for urban observations of WMO (2008). At the
210 compact midrise site of KAS, wind speeds and directions are measured using a 5 m mast placed
211 above a 20 m tall building. The open midrise site of SMA (Zürich-Fluntern) fulfils the "open
212 country" standard exposure guidelines (WMO, 2008), where a mast of 10 m is extending above
213 ground level. This height is considered sufficient in urban districts with low element height and
214 density (WMO, 2008).

215 No flux measurements were available for the studied period. We note that CCLM coupled with
216 DCEP has already been validated with data from the Basel Urban Boundary Layer Experiment
217 (BUBBLE) field campaign (Rotach *et al.*, 2005) by Schubert and Grossman-Clarke (2014). They
218 found a good online performance of the model system, comparable with other urban canopy
219 models.

220 Specific urban canopy parameters have to be derived at each atmospheric model grid cell in the
221 domain, at different model resolutions. High-resolution datasets were used in this study to avoid
222 loss of information during interpolation. The Degree of Soil Sealing 2009 (EEA, 2010) dataset
223 with 20 m spatial resolution has been used to derive the fraction of urban surfaces ($f_{urb}$). Input
224 data such as surface fraction covered by buildings ($f_{build}$), building height distribution (γ), build-
225 ing and street width distribution ($W_{build}$, $W_{street}$) are derived from a 3D building model

(Swisstopo, 2010) covering the entire domain with a level of detail (LoD) of 1. Details on the derivation of the urban canopy parameters are provided in the Appendix.

The anthropogenic heat flux ($AHF$) was neglected in this study, as its contribution is relatively small in summer compared to the net radiative forcing $R^*$. Studies on European cities located in similar climatic areas estimated an $AHF$ of 10-20 W m$^{-2}$ during summertime (Christen and Vogt, 2004; Klysik, 1996; Masson *et al.*, 2008), corresponding to only 2-4 % of the period averaged daily maximum $R^*$.

## 2.4 Evaluation methodology

In order to ensure a robust comparison at different model resolutions, the model results were compared to a defined area associated with each observation location, called here *evaluation frame*. The evaluation frame corresponds to the 1 km$^2$ area of the grid cell enclosing the site at the coarsest model resolution (Figure 3 , blue square). For high-resolution results, it includes all grid cells contained within and overlapping with that coarse grid cell (Figure 3 , solid black lines). Since the grids are not perfectly aligned, the frame is somewhat larger at the highest resolution (1.56 km$^2$). Within the evaluation frame, the maximum, minimum and mean values are calculated, together with the value of the grid cell containing the observation location. We remark that for all horizontal resolutions the vertical resolution remains the same, so all values are evaluated at the same height equal to the station height.

The evaluation frame allows comparing values averaged over approximately the same area and, therefore, enables analysing more correctly the dependence of spatially averaged quantities on model resolution. In addition, the influence of loss of variability at lower resolution can be quantified allowing for better understanding the advantage of high resolution for urban climate applications at local scale.

# 3. Results

## 3.1 Urban canopy parameters

Figure 4 shows the distribution of the urban fraction and building fraction for the Zurich area, and their corresponding variance, for different resolutions. We observe that, in general, the heterogeneity of urban parameters increased from large to small grid spacing. The variance of the fraction of urban surfaces $f_{urb}$ and building surfaces $f_{build}$ almost doubled from 1 km to 250 m resolution.

The value of $f_{urb}$ and $f_{build}$ generally increased from large to small grid spacing at compact midrise sites, whereas it decreased at open midrise sites (Table 1). This response is not seen at all sites since occasionally a site may become more (or less) urban at the next higher resolution and less urban again at even higher resolution depending on the specific surroundings of the site (e.g. $f_{urb}$ at SCH).

The distribution of street canyon directions changed only moderately between the different sites with NE-SW being the predominant direction (Table 2, data only represented for the 250 resolution).

## 3.2 Air temperature

The time evolution of air temperature over the 18 days for the different sites is shown in Figure S1. We observe that the performance of CCLM-DCEP remains constant throughout the entire heat wave event. An important model bias was found at the rural station REH during night-time, where the model overestimates the observed temperature in all configurations. This disagreement is attributed to the fact that CCLM is not able to reproduce the very low turbulent fluxes that occur during very stable boundary layer conditions. The inability of CCLM in representing very stable conditions has been already pointed out by Buzzi *et al.* (2011) and it remains still an open challenge for weather and climate models in general (Holtslag *et al.*, 2013).

The simulated mean diurnal cycle of air temperature for the different model resolutions averaged over the full 18-days period is shown in Figure 5 (a-b) for urban (compact and open midrise), together with the corresponding urban heat island intensity (Fig. c-d). The UHI intensity is defined as $T_{MOD\_urb} - T_{OBS\_rur}$ , where $T_{MOD\_urb}$ is the modelled temperature at the urban site of KAS (used as reference) and $T_{OBS\_rur}$ is the observed temperature at the rural site of REH. Observed temperature at the rural site is used in order not to introduce the systematic model night-time bias mentioned above in the calculation of the UHI intensity.

CCLM-DCEP results mostly matched the observations during night-time, while an overestimation of the daytime air temperature of up to 2 °C for compact midrise sites and 1 °C for open midrise sites was found. Noticeable is a tendency of CCLM-DCEP to produce a too rapid temperature rise in the morning and a too early decline in the late afternoon. As a result, the maximum 2-m air temperature was reached about 2 hours too early, and a significant warm bias appeared particularly between 10 and 13 local time. These differences led to a too high UHI intensity during daytime and a delayed UHI increase in the evening (Figure 5 (c,d)). This behaviour was already observed by Schubert and Grossman-Clarke (2014) and attributed to a general warm bias of the CCLM model, though further work will be needed in the future to fully disclose the mechanisms.

The Figure 5 (a,b) further indicate that CCLM-DCEP showed better agreement with observed air temperatures than CCLM-STD during night-time and late afternoon at all the model resolutions. Differences in temperature between CCLM-DCEP and CCLM-STD in the city centre, i.e. at compact midrise sites, are of the order of 1.2°C at night and 0.5-0.8°C during the day. In the CCLM-DCEP results at all model resolutions, compact midrise locations showed a 1°C higher night-time minimum air temperature than open midrise locations (Figure 5). A similar behaviour was not seen for the standard CCLM, where almost no difference was found between compact and open midrise sites.

Figure 5 shows that the CCLM-DCEP simulations at 500 m and 1 km resolution collapsed in the range of variability of the 250m simulation over the evaluation frame. The range of variability in the evaluation frame was found to be larger than the difference between results at different model resolutions. This suggests that the parameterisation used in DCEP have little (or no) scale dependency, i.e. DCEP can be used at different model resolutions (in the range 250 m – 1 km) without affecting the performance. A variability of air temperature as high as 2°C during daytime and 1°C during night-time was found in the evaluation frame, with higher values at open than at compact midrise sites. The air temperature variability was largest around noon and relatively small in the early morning hours (6 to 9 local time).

Statistical scores for all the simulations are shown in Table 3. A higher resolution produced a reduced mean bias error (MBE) only for open midrise sites of STA and ROS. At the compact midrise sites (KAS and SCH), low-resolution simulations showed better scores in terms of MBE. In terms of root-mean-square error (RMSE), we found no systematic change with model resolution.

Figure 6 shows the spatial distribution of period-averaged 2 m air temperatures using CCLM-STD and CCLM-DCEP at the different spatial resolutions for the conditions in the early morning (6 LT) and mid-afternoon (15 LT), which approximately corresponded to the time of the daily minimum and maximum temperatures, respectively.

In CCLM-DCEP, the entire urban area assumed an almost uniform temperature during night-time, while hot spots were found during daytime. Comparing Figure 4 and 6, we observe that during daytime, the hot spots (Figure 6 b) were localized over areas with high urban fractions (Figure 4). The CCLM-DCEP results further suggested a cooling effect of the lake on the surrounding portion of the urban area during daytime. In CCLM-STD, we found no significant variation between daytime and night-time.

## 3.3 Surface heat fluxes

In order to understand the causes of the spatial and temporal variability of the simulated air temperature, the surface heat fluxes are investigated. Specifically, the net incoming radiation ($R^*$), the sensible heat flux ($SHF$) and the latent heat flux ($LHF$) are analysed here. $SHF$ and $LHF$ are considered positive if the energy flows from the surface to the atmosphere.

Figure 7 shows the simulated period-averaged diurnal cycle of energy fluxes at the compact and open midrise sites at different horizontal grid spacing. At compact midrise sites, more energy was released as sensible heat than at open midrise sites. Within the urban area, sensible heat fluxes reached values up to 400 W $m^{-2}$ and vary spatially by more than 100 W $m^{-2}$ during day-time (Figure 8). During night-time (Figure 8 a), compact midrise sites maintained small positive values of sensible heat flux up to 50 W $m^{-2}$, while the values in open midrise sites were very low and almost 0 W $m^{-2}$. Spatial differences between adjacent grid cell values of up to 20 W $m^{-2}$ were observed during night-time.

The response of the sensible heat flux to model grid spacing was rather small, with an average variation of about 7% (~20 W $m^{-2}$) between model resolutions during daytime (Figure 7).

The latent heat fluxes in Figure 7 reached values up to 200 W $m^{-2}$ during daytime, while during night-time LHF was almost zero indicating less evaporation and almost no transpiration. Figure 8 shows that LHF during daytime was lower within urban compact midrise areas (around 100 W $m^{-2}$) and higher in open midrise areas (200 W $m^{-2}$).

$LHF$ shows a quite large sensitivity to model resolution (Figure 7), with differences between model resolutions of more than 25% (50 W $m^{-2}$) during daytime. Generally, lower values of $LHF$ were found at finer grid spacing. This behaviour is in accordance with the high range of variability of $LHF$ in the evaluation frame (Figure 7) and with Table 2, where higher values of urban fraction $f_{urb}$ are associated with finer grid spacing.

Figure 7 shows the net incoming radiation, which is considered positive if the energy flows from the atmosphere to the surface. $R^*$ does not show considerable differences between compact and open midrise. During daytime, values varied spatially between 550 and 600 W $m^{-2}$, while during night-time values between -60 and -90 W $m^{-2}$ were reached. Figure S3 shows the spatial variation of $R^*$ inside the urban area. Comparing Figure S3 and Figure 4 shows that $R^*$ was determined more by the building fraction than the urban fraction. For completeness, the spatial variation of net incoming longwave and shortwave radiation is also shown in Figure S4 and S5, respectively. Comparing of Figure S5 and Figure 4 shows that less net short wave radiation was received in areas with higher buildings, because of building shading effects. Variations of up to about 8 % (50 W $m^{-2}$) of the net incoming shortwave radiation were found in the urban area. During night-time, $R^*$ shows a less homogeneous behaviour than during daytime with differences up to about 30% (30 W $m^{-2}$) between two neighbouring grid cells (see Figure S2). For completeness, we show also in the Supporting Information the storage flux which is defined as $Stor \cong R^* - SHF - LHF$ (Figure S3). We observed during daytime storage fluxes up to 225 W $m^{-2}$ especially in region with high urban fraction (compact midrise), while during night-time these areas show fluxes of -100 W $m^{-2}$.

## 3.4 Wind speed

The measured and simulated period-averaged diurnal cycle of wind speed is shown in Figure 9. The comparison with observed wind speed shows a slight overestimation but overall a very good correlation for both sites. CCLM-DCEP did not improve the performance compared to CCLM-STD. At the observation locations, the period-averaged wind speeds tended to increase with model resolution (Figure 9). This behaviour was most evident during daytime. We found a high spatial variability of the mean winds of up to 2 m $s^{-1}$ during daytime in the evaluation frame (Figure 9). Figure S6 in the Supporting Information shows a comparison between simulated and measured wind speeds at the different observation sites during the entire 18-days period. In

general, we found a good agreement with some extreme values only captured at high resolution. Figure 10 shows the period-averaged spatial distribution of 10-m wind speed at 06 LT and 15 LT simulated with CCLM-DCEP. Wind speeds were rather low in the night reaching values of 1 m $s^{-1}$ and increasing in the afternoon reaching values up to 5 m $s^{-1}$. Within the urban area, we simulated wind speed differences up to 2 m $s^{-1}$ and 1 m $s^{-1}$ during daytime and night-time, respectively. These differences were more evident at high resolution where variations in urban morphology (such as building height distribution) inside the urban area became more resolved (Figure 10). Specifically, we found higher wind speeds (+~1 m $s^{-1}$) during daytime over the large open space of the railway tracks where the flow encountered no vertical obstacles (Figure 10).

# 4. Discussion

## 4.1 Impact of resolution

The values of $f_{urb}$ and $f_{build}$ increased from large to small grid spacing at compact midrise sites and decrease at open midrise sites. This indicates a better local representation of the site characteristic (e.g. fraction of urban surfaces and building density). Small-scale urban features such as rivers and urban parks start to be resolved at the highest model resolution of 250 m, and topographic features such as lake boundaries and orography are better represented. The variations of $f_{urb}$ and $f_{build}$ with model resolution had a direct impact on the surface heat fluxes, specifically on $LHF$. $LHF$ was found to be very sensitive to model grid spacing, as found also by Flagg and Taylor (2011). We found lower values of $LHF$ at the observation sites at finer grid spacing because natural patches that surround the urban area were not included anymore in the finer grid cell. This behaviour was confirmed by the high range of variability of $LHF$ in the evaluation frame (Figure 7) and by Table 2, where higher values of urban fraction $f_{urb}$ are associated with finer grid spacing. In comparison with $LHF$, the other surface energy fluxes ($SHF$ and $R^*$) showed a rather low sensitivity to model resolution. We remark that in our simulations all build-

395 ings in the city had the same roof and wall albedos which could explain the lower sensitivity of
396 $SHF$ and $R^*$ to model resolution. When different values of albedo are used, a higher sensitivity
397 to resolution might be expected.

398 The comparison between measurements and simulations shows that model resolution improved
399 model performance only at open midrise sites, while an overestimation of daytime air tempera-
400 ture was found over compact midrise sites. However, this observation has to be considered with
401 care. There was indeed a considerable spread in temperatures at 250 m resolution within a sin-
402 gle grid cell of the 1 km simulation, suggesting that the agreement between the different reso-
403 lutions could be influenced by the representativeness of the observation sites. In other words,
404 the grid cell where an observation site is contained may not be the most representative of the
405 site itself.

406 We found a rather small scale dependency of CCLM-DCEP when simulating air temperatures,
407 likely owed to the physically-based representation of street canyons in DCEP and to the ap-
408 proach of representing a single grid cell as a statistical ensemble of street orientations and
409 buildings.

410 The increase in wind speed with model resolution is attributed to the larger horizontal pressure
411 gradients produced at higher resolution, as a consequence of higher temperature gradients and
412 more pronounced orography. The slight overestimation of wind speed at high resolution is
413 probably related to the overestimation of daytime air temperature.

414 To shed further light on the question, how realistic intra-urban gradients in temperature, wind
415 speed and energy fluxes are represented in high-resolution simulations, a denser network of
416 temperature and wind observations and additional measurements of energy fluxes from flux
417 towers or airborne measurements would be required. Such comprehensive datasets are only
418 available from very few observations campaigns (Muller *et al.*, 2013).

## 4.2 Representation of intra-urban climates

CCLM-DCEP was able to reproduce the temperature differences between compact and open midrise sites during the evaluation period. We found a spatial variability in air temperature as high as 2°C during daytime and 1°C during night-time in the evaluation frame, with higher values at open than at compact midrise sites. The observed large temperature variability in the evaluation frame was due to the strong heterogeneity in land use parameters for open midrise sites, where small-scale features such as rivers and urban parks started to be resolved. The air temperature variability was larger during daytime, while it was small during transition times, especially in the morning. During daytime, hot spots with high air temperature (Figure 6 b) were localized over areas with high urban fractions (Figure 4) where higher sensible heat fluxes were produced (Figure 8 b). The cooling effect of the lake was only evident during daytime when the temperature difference between lake and land surface temperature was largest.

The heterogeneity in urban parameters had noticeable effects on the energy fluxes partitioning. The greater amount of energy released as sensible heat flux in compact midrise sites has also been found in other experimental (Rotach *et al.*, 2005) and modelling (Loridan *et al.*, 2013) studies. The higher sensible heat flux was driven by a higher urban fraction $f_{urb}$ (and correspondingly lower vegetation fraction $f_{nat}$) and by differences in the values of the urban canopy parameters (Table 2).

We found a strong wind speed variability of up to 2 m $s^{-1}$ during daytime and up to 1 m $s^{-1}$ during night-time in the evaluation frame (Figure 9). This variability was produced by local variations in terrain height and urban morphology (Figure 4). However, we found no one-to-one relation between the temperature and the wind speed spatial distribution.

## 5. Conclusions

This study investigates the potential of exploiting a mesoscale model for local urban scale climate simulations. The weather and climate model CCLM, coupled with the multi-layer urban canopy model DCEP, was used at increasing model resolution from 1 km to 250 m grid spacing. We assessed the impact of model resolution on the simulated air temperature, surface energy fluxes and wind speed during the heat wave event of June-July 2015 in Zurich (Switzerland).

The heterogeneity of the urban canopy parameters strongly increased with model resolution, where an almost doubled variance of these parameters was observed. Small-scale features such as urban parks, large railways and districts with peculiar urban morphology started to be resolved at sub-kilometre resolution. Large-scale features such as lake boundaries and orography were also better resolved.

CCLM-DCEP was found to better represent the different air temperature daily profiles as observed in compact midrise and open midrise sites compared to the standard CCLM. Specifically, CCLM-DCEP better resolved the higher night-time minimum air temperature in compact midrise locations.

An air temperature variability as high as 2°C during daytime and 1°C during night-time was found over a 1 km x 1 km evaluation frame, at 250 m resolution. We also found that the mean values of 2-m air temperature over the evaluation frame area remain conserved, i.e. the model resolution (from 1 km to 250 m) does not affect the performances of the urban parameterisation.

Latent heat flux (LHF) was found to be very sensitive to model resolution, with differences of up to 50 W $m^{-2}$ (25 %) between the different model grid spacing. Lower values of LHF were found at finer grid spacing where surrounding natural patches are not included in the grid cell. At compact midrise sites, more energy was released as sensible heat flux (SHF) than at open mid-

rise sites. These variations were driven by a higher urban fraction and correspondingly lower vegetation fraction and by differences in the values of the urban canopy parameters.

Regarding wind speed, CCLM-DCEP did not substantially improve the agreement with observations compared to the standard CCLM. Higher values of wind speed were modelled at higher resolution in correlation with higher pressure gradients generated between the city and the surroundings. As for the other variables, we observed an increase in variability with model resolution. Within the urban area, we simulated a difference up to 1.5 m $s^{-1}$ and 1 m $s^{-1}$ during daytime and night-time, respectively.

The results show that CCLM-DCEP has the potential to represent the urban climate at the local (or neighbourhood) scale when used at high (sub-kilometre) resolution. Sub-kilometre resolution allows better representing urban features such as urban parks, rivers, large railways and districts with peculiar urban morphology (e.g. old city cores). Urban simulation at local scale has the potential to better support applications such as urban planning, building energy use and urban air quality. The results of this study extend to similar modelling system such as WRF/urban (Chen et al. 2011), when used with highly physical multi-layer urban canopy models.

## Acknowledgements

The study is funded by Empa. We thank MeteoSwiss, the Federal Office for Environment of Switzerland (BAFU), Empa and Ostluft for providing meteorological observations. MeteoSwiss is also acknowledged for providing the meteorological analysis. The use of Empa's computational resources is greatly acknowledged.

## Appendix

The derivation of the urban canopy parameters used in CCLM-DCEP is described here. It partially follows the methodology proposed by Schubert and Grossman-Clarke (2014).

The urban fraction $f_{urb}$, defined as the planar fraction of urban surfaces in a model grid cell, is derived from the "Degree of Soil Sealing 2009" dataset with 20 m spatial resolution (EEA 2010). The degree of soil sealing is used as a proxy for the urban fraction, as done in previous studies (e.g Wouters *et al.* (2015)). The high resolution data is interpolated on the CCLM grid at the different model grid spacing (1 km, 500 m, 250 m).

The building fraction $f_{build}$, defined as the planar fraction of buildings in a model grid cell, is calculated from a 3D building model (Swisstopo, 2010) covering the entire domain with a level of detail (LoD) of 1. In LoD 1, buildings are represented by block models where roof details are not included. The street fraction $f_{str}$ is then derived, given that $f_{str} = f_{urb} - f_{build}$. It should be noted that vegetation in the street canyon (e.g. street trees or small gardens) is not considered in the current DCEP version, i.e. the urban part of the grid cell is completely covered by street and building surfaces.

The direction of the street canyon influences the shadowing of the urban surfaces and the drag forces on the walls (e.g. drag forces do not act on the walls if the street canyon is aligned with the direction of the average wind speed). Thus, all urban radiative properties and fluxes are averaged, weighted with the fraction $f_{dir}$ of the corresponding street direction. In this study, 4 street canyon orientation classes are used: namely Northwest-Southeast (NW-SE), North-South (N-S), Northeast-Southwest (NE-SW), and East-West (E-W). In order to calculate $f_{dir}$ of every mesoscale grid cell, the distribution of canyon angles of all wall polygons in the 3D building model is weighted with their respective wall area.

The building height probability $\gamma\ (z)$ is determined by the distribution of building heights in the 3D building model weighted by the respective wall area of the building. A building height is assigned to a street direction depending on the street direction of its wall surfaces.

The street width $W_{str}$, defined as the average width (in metres) of the street of a certain canyon orientation class, is calculated using the flowing empirical equation:

$$W_{str} = 5\text{m} + f_{str} \times 45\text{m}. \quad \text{(A1)}$$

$W_{str}$ can therefore assume values from 5 to 50 m, corresponding to the minimum and maximum values of street width observed in Zurich, respectively. Equation 2 is derived based on a citywide mean $W_{str}$ of 20 m (corresponding to a $f_{str}$ of 0.33) and a direct correlation between $W_{str}$ and $f_{str}$ is assumed. Considering that the urban part of the grid cell is completely covered by street and building surfaces, the building width $W_{build}$ is given by:

$$W_{build} = \frac{f_{build}}{f_{str}} W_{str} ., \quad \text{(A2)}$$

## Bibliography


Arnfield AJ. 2003. Two decades of urban climate research: A review of turbulence, exchanges of energy and water, and the urban heat island. *International Journal of Climatology* **23**(1): 1–26. DOI: 10.1002/joc.859.

Buwen D, Sutton R, Shaffrey L, Wilcox L. 2016. The 2015 European Heat Wave. *Bulletin of the American Meteorological Society* **97**(12): S57-62. DOI: 10.1175/BAMS-D-12-00021.1.

Buzzi M, Rotach MW, Holtslag M, Holtslag AAM. 2011. Evaluation of the COSMO-SC turbulence scheme in a shear-driven stable boundary layer. *Meteorologische Zeitschrift* **20**(3): 335–350. DOI: 10.1127/0941-2948/2011/0050.

Chen F, Bornstein R, Grimmond S, Li J, Liang X, Martilli A, Miao S, Voogt J, Wang YH. 2012. Research priorities in observing and modeling urban weather and climate. *Bulletin of the American Meteorological Society* **93**(11): 1725–1728. DOI: 10.1175/BAMS-D-11-00217.1.

Chen F, Kusaka H, Bornstein R, Ching J, Grimmond CSB, Grossman-Clarke S, Loridan T, Manning KW, Martilli A, Miao S, Sailor D, Salamanca FP, Taha H, Tewari M, Wang X, Wyszogrodzki AA, Zhang C. 2011. The integrated WRF/urban modelling system: Development, evaluation, and applications to urban environmental problems. *International Journal of Climatology* **31**(2): 273–288. DOI: 10.1002/joc.2158.

Christen A, Vogt R. 2004. Energy and radiation balance of a central European city. *International Journal of Climatology* **24**: 1395–1421. DOI: 10.1002/joc.1074.

Doms G, Förstner J, Heise E, Herzog H-J, Mironov D, Raschendorfer M, Reinhardt T, Ritter B, Schrodin R, Schulz J-P, Vogel G. 2011. *A Description of the Nonhydrostatic Regional COSMO Model Part II: Physical Parameterization*. Offenbach, Germany.

EEA. 2010. *EEA Fast Track Service Precursor on Land Monitoring - Degree of soil sealing*. Kongens Nytorv 6, 1050 Copenhagen, Denmark.

FAO, IIASA, ISRIC, ISS-CAS, JRC. 2009. *Harmonized World Soil Database (version 1.1). FAO, Rome, Italy and IIASA, Laxenburg, Austria*.

549 Flagg DD, Taylor PA. 2011. Sensitivity of mesoscale model urban boundary layer meteorology to
550 the scale of urban representation. *Atmospheric Chemistry and Physics* **11**(6): 2951–2972. DOI:
551 10.5194/acp-11-2951-2011.
552 Giorgi F, Avissar R. 1997. Representation of heterogeneity effects in Earth system modeling:
553 Experience from land surface modeling. *Reviews of Geophysics* **35**(4): 413–437. DOI:
554 10.1029/97RG01754.
555 Grawe D, Thompson HL, Salmond JA, Cai XM, Schlünzen KH. 2013. Modelling the impact of
556 urbanisation on regional climate in the Greater London Area. *International Journal of*
557 *Climatology* **33**(10): 2388–2401. DOI: 10.1002/joc.3589.
558 Grossman-Clarke S, Schubert S, Fenner D. 2017. Urban effects on summertime air temperature in
559 Germany under climate change. *International Journal of Climatology*. John Wiley & Sons, Ltd
560 **37**(2): 905–917. DOI: 10.1002/joc.4748.
561 Holtslag AAM, Svensson G, Baas P, Basu S, Beare B, Beljaars ACM, Bosveld FC, Cuxart J, Lindvall J,
562 Steeneveld GJ, Tjernström M, Van De Wiel BJH, Holtslag AAM, Svensson G, Baas P, Basu S, Beare
563 B, Beljaars ACM, Bosveld FC, Cuxart J, Lindvall J, Steeneveld GJ, Tjernström M, Wiel BJH Van De.
564 2013. Stable Atmospheric Boundary Layers and Diurnal Cycles: Challenges for Weather and
565 Climate Models. *Bulletin of the American Meteorological Society*. American Meteorological
566 Society **94**(11): 1691–1706. DOI: 10.1175/BAMS-D-11-00187.1.
567 Ionita M, Tallaksen LM, Kingston DG, Stagge JH, Laaha G, Lanen HAJ Van, Scholz P, Chelcea SM,
568 Haslinger K. 2017. The European 2015 drought from a climatological perspective. *Hydrology and*
569 *Earth System Sciences* **21**: 1397–1419. DOI: 10.5194/hess-21-1397-2017.
570 Klysik K. 1996. Spatial and seasonal distribution of anthropogenic heat emissions in Lodz,
571 Poland. *Atmospheric Environment* **30**(20): 3397–3404. DOI: 10.1016/1352-2310(96)00043-X.
572 Leutwyler D, Fuhrer O, Lapillonne X, Lüthi D, Schär C. 2016. Towards European-scale convection-
573 resolving climate simulations with GPUs: a study with COSMO 4.19. *Geoscientific Model*
574 *Development*. Copernicus GmbH **9**(9): 3393–3412. DOI: 10.5194/GMD-9-3393-2016.
575 Li D, Bou-Zeid E. 2014. Quality and sensitivity of high-resolution numerical simulation of urban
576 heat islands. *Environmental Research Letters*. IOP Publishing **9**: 55002. DOI: 10.1088/1748-
577 9326/9/5/055002.
578 Li XX, Koh TY, Entekhabi D, Roth M, Panda J, Norford LK. 2013. A multi-resolution ensemble
579 study of a tropical urban environment and its interactions with the background regional
580 atmosphere. *Journal of Geophysical Research Atmospheres* **118**(17): 9804–9818. DOI:
581 10.1002/jgrd.50795.
582 Loridan T, Grimmond CSB. 2012. Multi-site evaluation of an urban land-surface model : intra-
583 urban heterogeneity , seasonality and parameter complexity requirements. *Quarterly Journal of*
584 *the Royal Meteorological Society* **138**(April): 1094–1113. DOI: 10.1002/qj.963.
585 Loridan T, Lindberg F, Jorba O, Kotthaus S, Grossman-Clarke S, Grimmond CSB. 2013. High
586 Resolution Simulation of the Variability of Surface Energy Balance Fluxes Across Central London
587 with Urban Zones for Energy Partitioning. *Boundary-Layer Meteorology* **147**(3): 493–523. DOI:
588 10.1007/s10546-013-9797-y.
589 Loveland TR, Reed BC, Brown JF, Ohlen DO, Zhu Z, Yang L, Merchant JW. 2000. Development of
590 a global land cover characteristics database and IGBP DISCover from 1 km AVHRR data.
591 *International Journal of Remote Sensing* **21**(6–7): 1303–1330. DOI: 10.1080/014311600210191.
592 Martilli A. 2007. Current research and future challenges in urban mesoscale modelling.
593 *International Journal of Climatology* **27**: 1549–1555. DOI: 10.1002/joc.1620.
594 Martilli A, Clappier A, Rotach MW. 2002. An urban surface exchange parameterization for
595 mesoscale models. *Boundary-Layer Meteorology* **104**: 261–304. DOI: 10.1023/A:1016099921195.

596 Masson V. 2006. Urban surface modeling and the meso-scale impact of cities. *Theoretical and*
597 *Applied Climatology* **84**(1–3): 35–45. DOI: 10.1007/s00704-005-0142-3.
598 Masson V, Gomes L, Pigeon G, Liousse C, Pont V, Lagouarde J, Voogt J. 2008. The Canopy and
599 Aerosol Particles Interactions in TOulouse Urban Layer ( CAPITOUL ) experiment. *Meteorology*
600 *and Atmospheric Physics* **102**: 135–157. DOI: 10.1007/s00703-008-0289-4.
601 Mellor GL, Yamada T. 1982. Development of a Turbulence Closure Model for Geophysical Fluid
602 Problems. *Reviews of Geophysics and Space Physics* **20**(4): 851–875. DOI:
603 10.1029/RG020i004p00851.
604 MeteoSwiss. 2017. *Climate normals Zürich/Fluntern*.
605 http://www.meteoswiss.admin.ch/product/output/climate-data/climate-diagrams-normal-
606 values-station-processing/SMA/climsheet_SMA_np8110_e.pdf (accessed 18-10-2017).
607 Miao SG, Chen F, Lemone MA, Tewari M, Li QC, Wang YC. 2009. An Observational and Modeling
608 Study of Characteristics of Urban Heat Island and Boundary Layer Structures in Beijing. *Journal*
609 *of Applied Meteorology and Climatology* **48**(3): 484–501. DOI: Doi 10.1175/2008jamc1909.1.
610 Muller CL, Chapman L, Grimmond CSB, Young T. 2013. Sensors and the city : a review of urban
611 meteorological networks. **1600**(February): 1585–1600. DOI: 10.1002/joc.3678.
612 Oleson KW, Bonan GB, Feddema J, Vertenstein M, Grimmond CSB. 2008. An Urban
613 Parameterization for a Global Climate Model. Part I: Formulation and Evaluation for Two Cities.
614 *Journal of Applied Meteorology and Climatology* **47**(4): 1038–1060. DOI:
615 10.1175/2007JAMC1597.1.
616 Ritter B, Geleyn J-F. 1992. A Comprehensive Radiation Scheme for Numerical Weather Prediction
617 Models with Potential Applications in Climate Simulations. *Monthly Weather Review* **120**: 303–
618 325. DOI: 10.1175/1520-0493(1992)120<0303:ACRSFN>2.0.CO;2.
619 Rockel B, Will A, Hense A. 2008. The Regional Climate Model COSMO-CLM ( CCLM ).
620 *Meteorologische Zeitschrift* **17**(4): 347–348. DOI: 10.1127/0941-2948/2008/0309.
621 Ronda RJ, Steeneveld GJ, Heusinkveld BG, Attema JJ, Holtslag AAM, Ronda RJ, Steeneveld GJ,
622 Heusinkveld BG, Attema JJ, Holtslag AAM. 2017. Urban fine-scale forecasting reveals weather
623 conditions with unprecedented detail. *Bulletin of the American Meteorological Society* (in press.).
624 DOI: 10.1175/BAMS-D-16-0297.1.
625 Rotach MW, Vogt R, Bernhofer C, Batchvarova E, Christen A, Clappier A, Feddersen B, Gryning
626 SE, Martucci G, Mayer H, Mitev V, Oke TR, Parlow E, Richner H, Roth M, Roulet YA, Ruffieux D,
627 Salmond JA, Schatzmann M, Voogt JA. 2005. BUBBLE - An urban boundary layer meteorology
628 project. *Theoretical and Applied Climatology* **81**(3–4): 231–261. DOI: 10.1007/s00704-004-0117-
629 9.
630 Roth M. 2011. *Urban heat islands*. *Handbook of Environmental Fluid Dynamics, Volume Two*. CRC
631 Press/Taylor & Francis Group, LLC. DOI: 10.1201/b13691-13.
632 Schraff CH. 1997. Mesoscale data assimilation and prediction of low stratus in the Alpine region.
633 *Meteorology and Atmospheric Physics*. Springer-Verlag **64**(1–2): 21–50. DOI:
634 10.1007/BF01044128.
635 Schubert S, Grossman-Clarke S. 2014. Evaluation of the coupled COSMO-CLM/DCEP model with
636 observations from BUBBLE. *Quarterly Journal of the Royal Meteorological Society* **140**(685): 2465–
637 2483. DOI: 10.1002/qj.2311.
638 Schubert S, Grossman-Clarke S, Martilli A. 2012. A Double-Canyon Radiation Scheme for Multi-
639 Layer Urban Canopy Models. *Boundary-Layer Meteorology* **145**(3): 439–468. DOI:
640 10.1007/s10546-012-9728-3.
641 Sharma A, Fernando HJS, Hamlet AF, Hellmann JJ, Barlage M, Chen F. 2017. Urban
642 meteorological modeling using WRF: a sensitivity study. *International Journal of Climatology*

**37**(4): 1885–1900. DOI: 10.1002/joc.4819.

Smiatek G, Rockel B, Schättler U. 2008. Time invariant data preprocessor for the climate version of the COSMO model (COSMO-CLM). *Meteorologische Zeitschrift* **17**(4): 395–405. DOI: 10.1127/0941-2948/2008/0302.

Steppeler J, Doms G, Schättler U, Bitzer HW, Gassmann A, Damrath U, Gregoric G. 2003. Meso-gamma scale forecasts using the nonhydrostatic model LM. *Meteorology and Atmospheric Physics*. Springer-Verlag **82**(1–4): 75–96. DOI: 10.1007/s00703-001-0592-9.

Stewart ID, Oke TR. 2012. Local climate zones for urban temperature studies. *Bulletin of the American Meteorological Society* **93**(12): 1879–1900. DOI: 10.1175/BAMS-D-11-00019.1.

Swisstopo. 2010. *swissBUILDINGS3D 1.0*. https://shop.swisstopo.admin.ch/en/products/landscape/build3D2 (accessed 18-10-2017)

Tiedkte M. 1989. A Comprehensive Mass Flux Scheme for Cumulus Parameterization in Large-Scale Models. *Monthly Weather Review* **117**: 1779–1800. DOI: 10.1175/1520-0493(1989)117<1779:ACMFSF>2.0.CO;2.

Trusilova K, Schubert S, Wouters H, Früh B, Demuzere M, Becker P. 2015. The urban land use in the COSMO-CLM model : a comparison of three parameterizations for Berlin. *Meteorologische Zeitschrift* **25**(2): 231–244. DOI: 10.1127/metz/2015/0587.

WMO. 2008. Guide to Meteorological Instruments and Methods of Observation, 7th edn. Instruments and Observing Methods Report No. 8. DOI: 10.1002/joc.3678

Wouters H, Demuzere M, Blahak U, Fortuniak K, Maiheu B, Camps J. 2016. The efficient urban canopy dependency parametrization ( SURY ) v1 . 0 for atmospheric modelling : description and application with the COSMO-CLM model for a Belgian summer. *Geoscientific Model Development* **9**: 3027–3054. DOI: 10.5194/gmd-9-3027-2016.

Wouters H, Demuzere M, DeRidder K, P.M.van Lipzig N. 2015. The impact of impervious water-storage parametrization on urban climate modelling. *Urban Climate* **11**: 24–50. DOI: 10.1016/J.UCLIM.2014.11.005.

# Tables

| | | |
|---|---|---|
| COSMO-CLM (CCLM) model (version 5) | Horizontal Grid Spacing | 1km, 500m, 250m |
| | Vertical resolution | 76 levels |
| | Urban parameterization | Bulk (STD)<br>DCEP |
| Input data | Boundary conditions | COSMO-2 analysis |
| | Urban fraction | Soil sealing 2 m res (EEA) |
| | Building data | LoD 1 building data (Local) |
| | Urban vegetation | LAI = 3, z0 = 0.1 m |

Table 1 - Resume of simulation details and input data.

| Site | Urban fraction $f_{urb}$ | | | Building fraction $f_{build}$ | | | Aspect ratio $H/W$ | | | Canyon direction (at 250m) | | | |
|---|---|---|---|---|---|---|---|---|---|---|---|---|---|
| | 1 km | 500m | 250m | 1 km | 500m | 250m | 1 km | 500m | 250m | NE-SW | N-S | NW-SE | E-W |
| KAS | 0.79 | 0.82 | 0.85 | 0.39 | 0.5 | 0.46 | 0.88 | 1.04 | 0.88 | 0.65 | 0.06 | 0.25 | 0.05 |
| SCH | 0.69 | 0.84 | 0.80 | 0.38 | 0.40 | 0.36 | 1.06 | 0.80 | 0.80 | 0.70 | 0.02 | 0.26 | 0.02 |
| STA | 0.54 | 0.58 | 0.57 | 0.32 | 0.24 | 0.30 | 0.95 | 0.69 | 0.82 | 0.44 | 0.17 | 0.17 | 0.22 |
| ROS | 0.65 | 0.6 | 0.54 | 0.35 | 0.37 | 0.31 | 0.77 | 0.92 | 0.88 | 0.62 | 0.09 | 0.21 | 0.08 |

Table 2 - Values of urban parameters at the grid cell corresponding to the observation sites for different horizontal grid spacing. Aspect ratio is the mean height-to-width ratio (H/W) of street canyons. Canyon direction represents the percentage of canyons with a specific direction and is only given for resolution 250 m.

| | | | **Air Temperature [°C]** | | | | | |
|---|---|---|---|---|---|---|---|---|
| Site | Description | Model | MBE | | | RMSE | | |
| | | | 1 km | 500m | 250m | 1 km | 500m | 250m |
| KAS | Urban, compact midrise | DCEP | 0.20 | 0.42 | 0.50 | 0.90 | 1.02 | 1.07 |
| | | STD | -0.60 | -0.50 | -0.57 | 1.07 | 1.02 | 1.07 |
| SCH | Urban, compact midrise | DCEP | 0.25 | 0.47 | 0.42 | 1.36 | 1.55 | 1.51 |
| | | STD | -0.54 | -0.53 | -0.54 | 1.51 | 1.62 | 1.60 |

| | | | | | | | | |
|---|---|---|---|---|---|---|---|---|
| STA | Urban, open midrise | DCEP | -0.27 | -0.09 | -0.09 | 1.34 | 1.38 | 1.38 |
| | | STD | -0.78 | -0.46 | -0.50 | 1.58 | 1.55 | 1.54 |
| ROS | Urban, open midrise | DCEP | -0.54 | -0.80 | -0.10 | 1.25 | 1.37 | 1.25 |
| | | STD | -0.89 | -0.64 | -0.44 | 1.39 | 1.34 | 1.29 |
| SMA | Urban, open low-rise | DCEP | 0.36 | 0.28 | 0.72 | 1.28 | 1.20 | 1.38 |
| | | STD | 0.02 | 0.08 | -0.11 | 1.23 | 1.17 | 1.17 |
| REH | Rural, low plants | DCEP | 0.62 | 0.73 | 1.03 | 1.60 | 1.65 | 1.81 |
| | | STD | 0.42 | 0.74 | 0.82 | 1.50 | 1.64 | 1.63 |

693

694 Table 3 - Period averaged mean-bias errors (MBE) and root-mean-square errors (RMSE) of the
695 air temperature at 2 m, calculated for the model grid cells in which the sites were situated. The
696 upper row for each site gives the values for CCLM-DCEP (DCEP), while the lower row lists the re-
697 sults for CCLM-STD (STD).

698

699

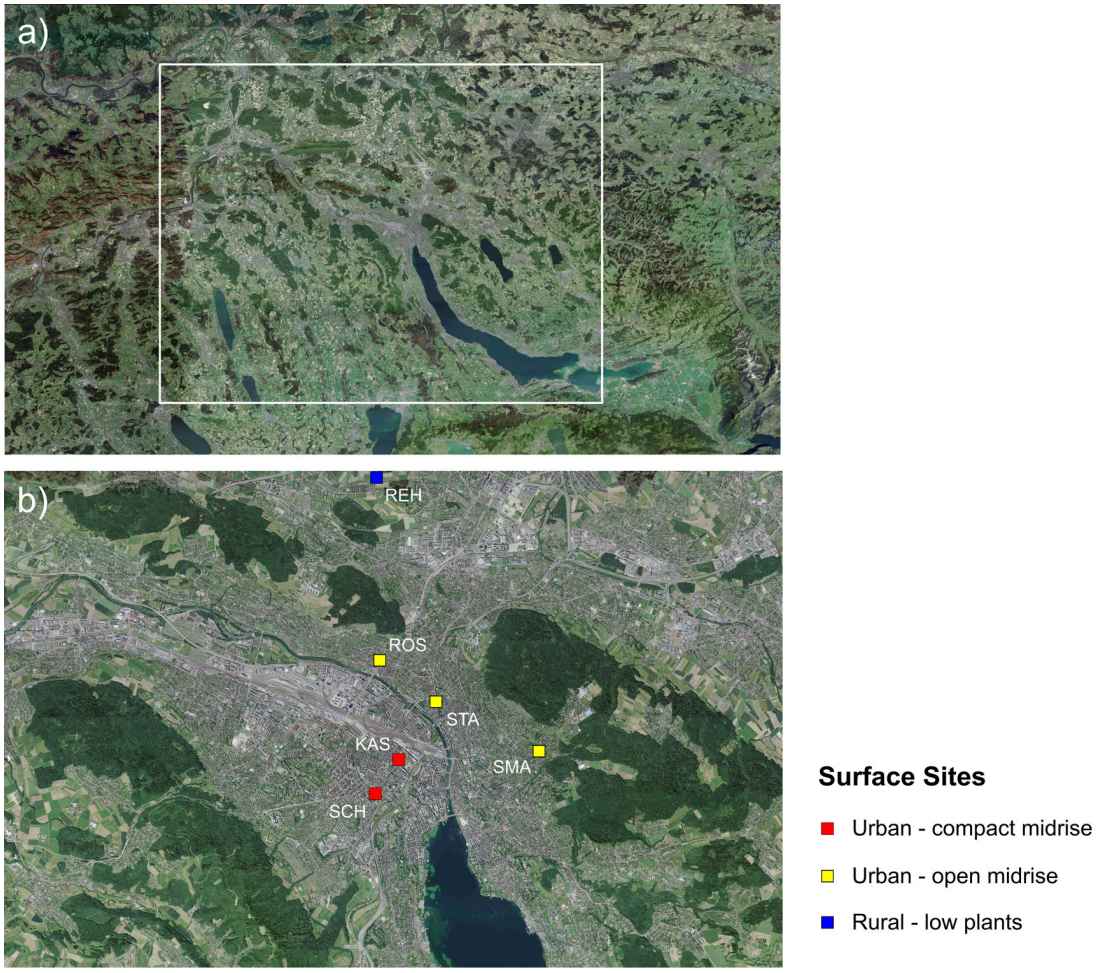


Figure 1 - Aerial views of the model domain (white rectangle) (a) and the city of Zurich with location of the sites used for model evaluation (b). Aerial photos reproduced by permission of SwissTopo (JA100120).

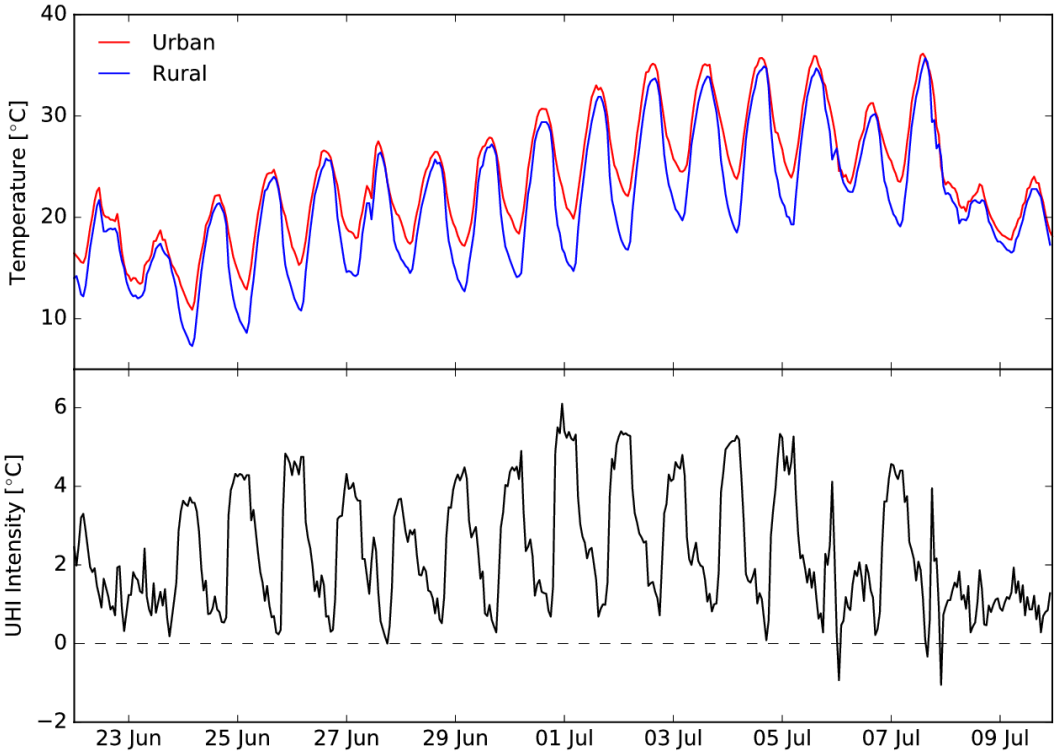


Figure 2 – Measured air temperature (2 m) at the sites of KAS (Urban) and REH (Rural) during the heat wave June 22 - July 10, 2015 (a). UHI intensity calculated as air temperature difference between the sites of KAS and REH (b).

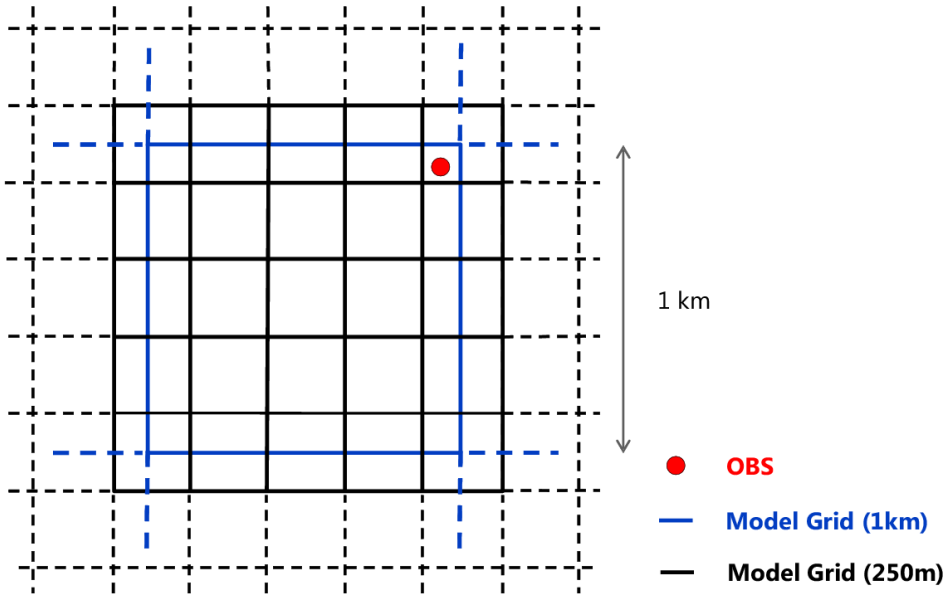


Figure 3 – Schematic of the evaluation methodology. OBS (in red) is the location of the observation site. The solid lines are the grid cells used for the comparison. Only 1 km (corresponding to the evaluation frame) and 250 m grid cells are shown for simplicity.

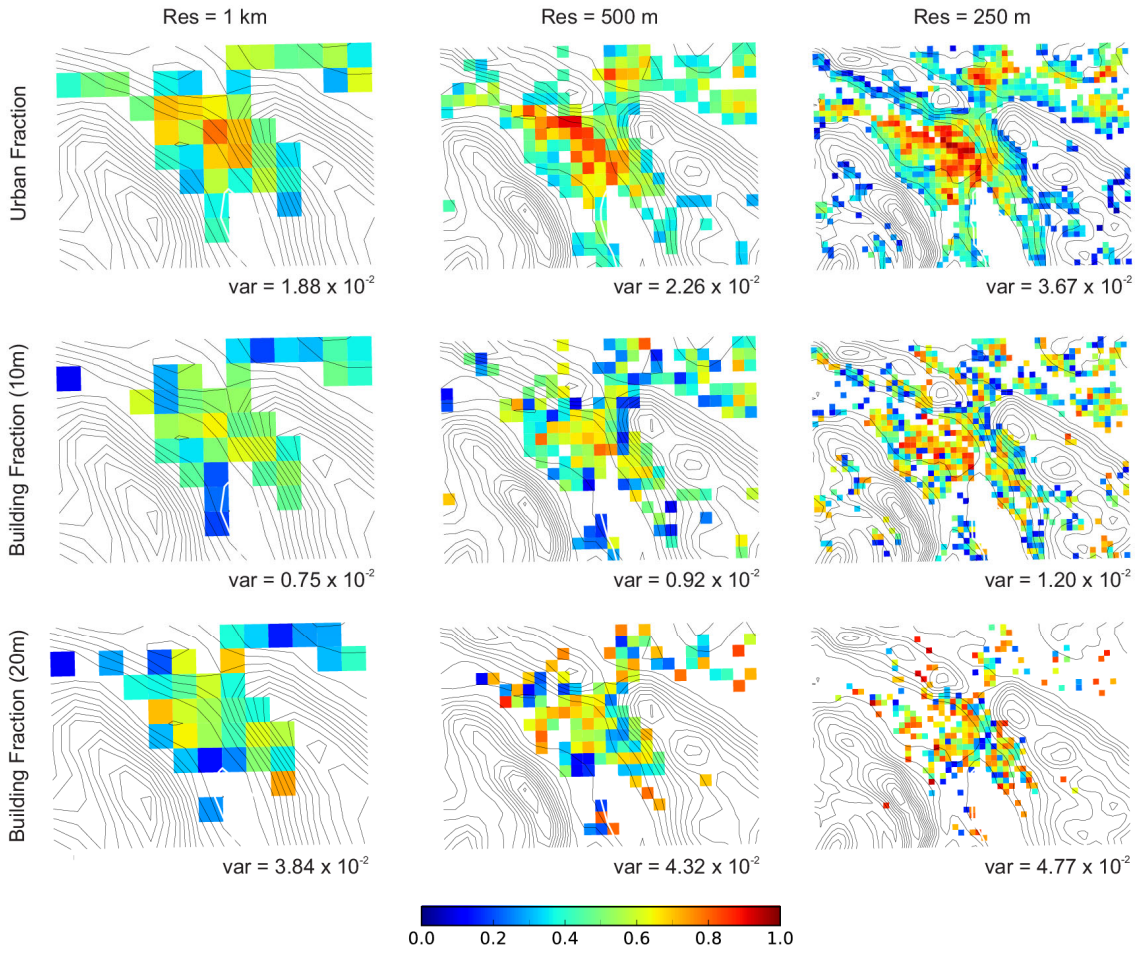


715

716 Figure 4 - Urban parameters for CCLM-DCEP derived for the model domain at the different hori-
717 zontal grid spacing: urban fraction, building fraction at the height of 10 m and building fraction
718 at the height of 20 m. The building fraction values are averaged over all considered street direc-
719 tions. The variances (var) are also reported. Only values higher than 0.1 are represented.

720

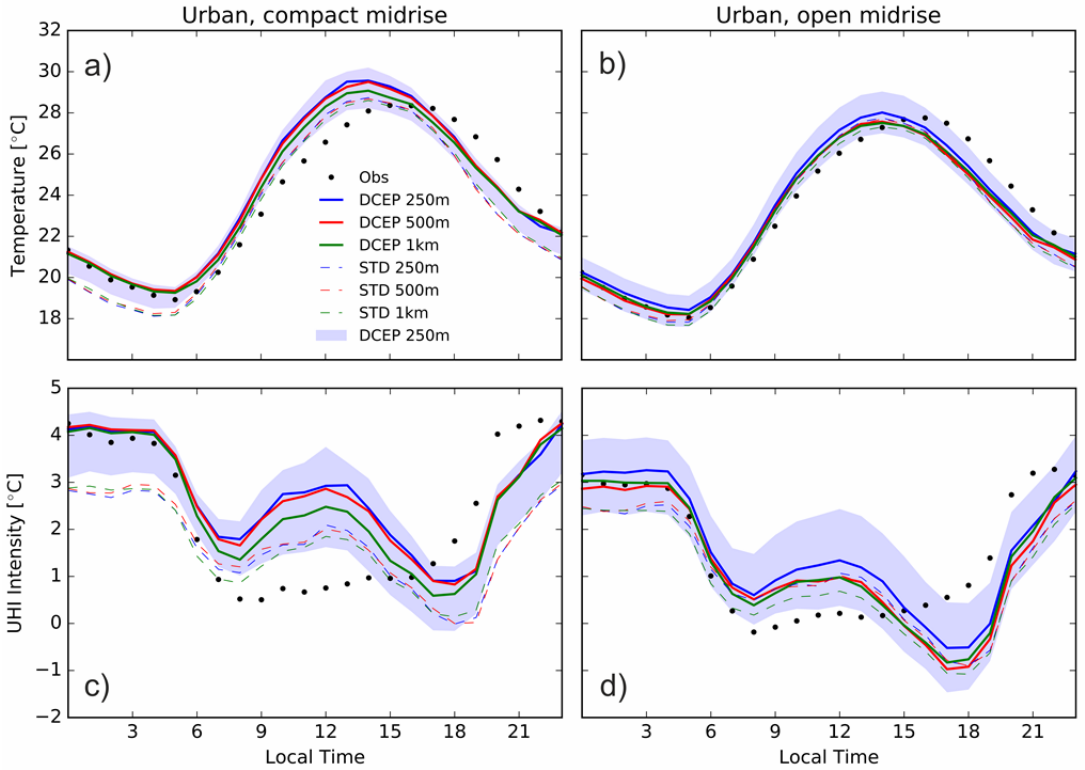


721

722 Figure 5 - Measured (Obs) and simulated average diurnal cycle of 2-m air temperature and UHI
723 intensity at the different horizontal grid spacings at compact (a, c) and open urban (b, d) sites.
724 The shaded area represents the range between minimum and maximum in the 250m CCLM-
725 DCEP simulation within the corresponding grid cell of the 1 km simulation. The results from the
726 STD simulation are also shown for comparison.

727

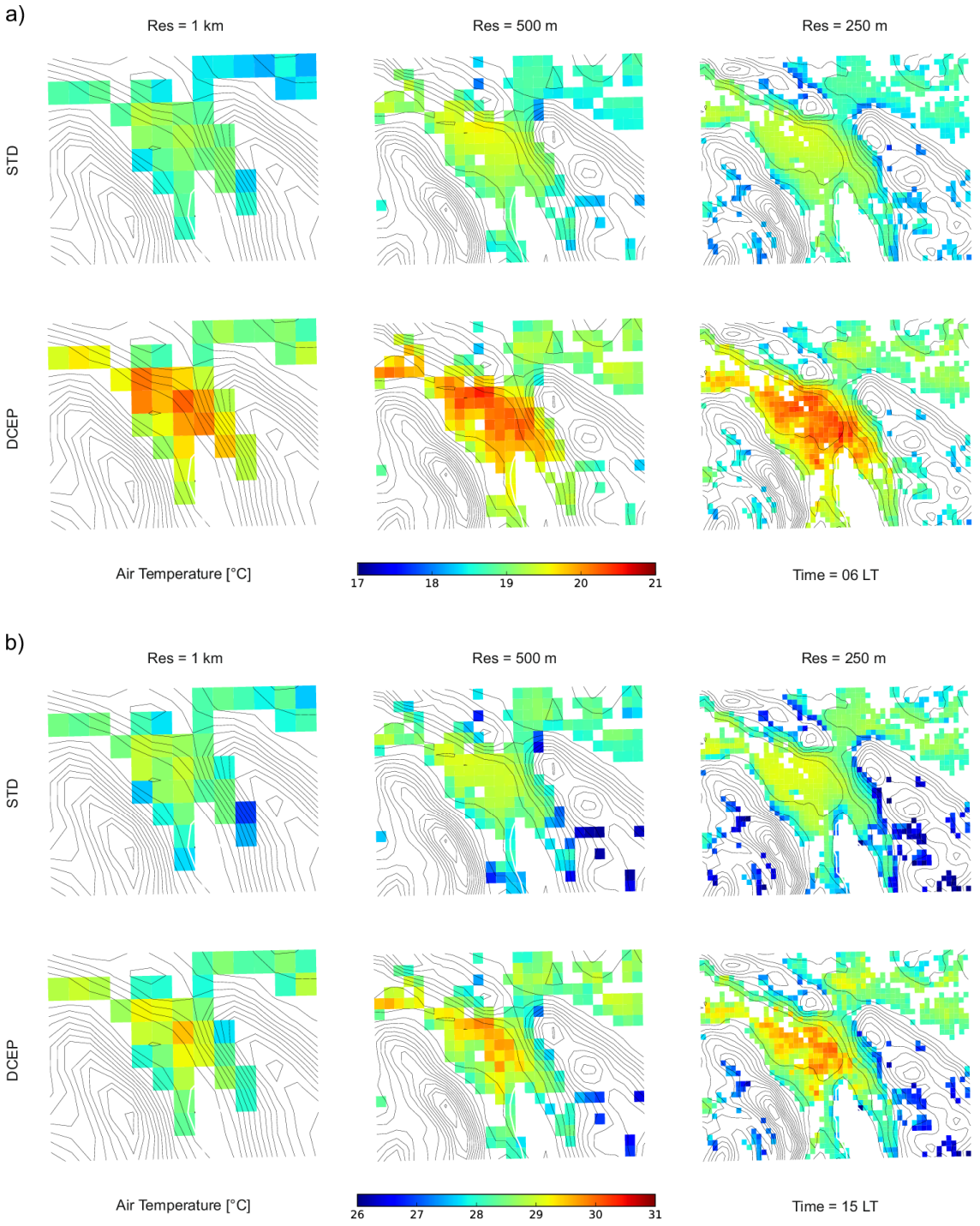


Figure 6- Spatial distribution of the simulated period-averaged 2-m air temperature [°C] at 06 LT (a) and 15 LT (b) using CCLM-STD (upper row) and CCLM-DCEP (lower row) urban parameterization with a grid spacing of 1 km, 500m and 250m (from left to right), respectively.

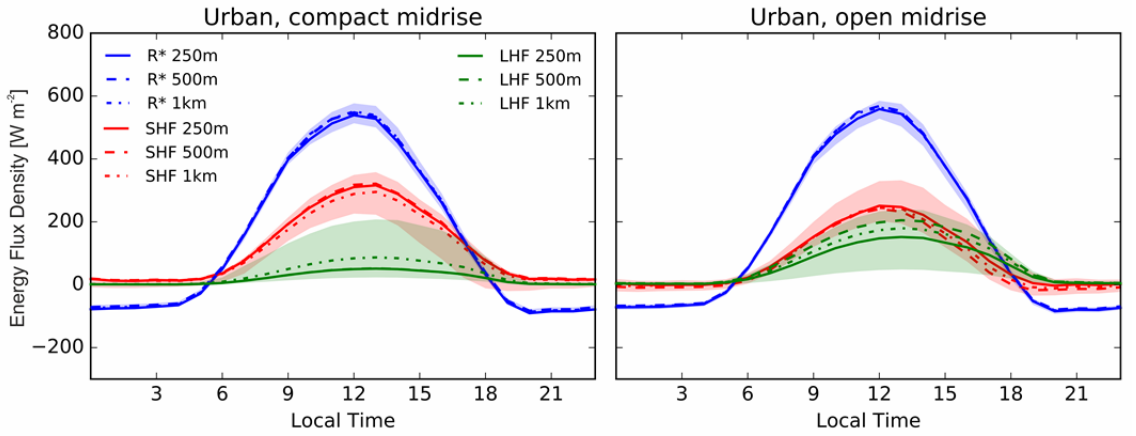


Figure 7 - Simulated average diurnal cycle of surface heat fluxes at the compact and open mid-rise sites at different horizontal grid spacing. Only results of the simulation with CCLM-DCEP are shown here. The shaded areas represent the range of variability of the energy fluxes of the 250m simulation only.

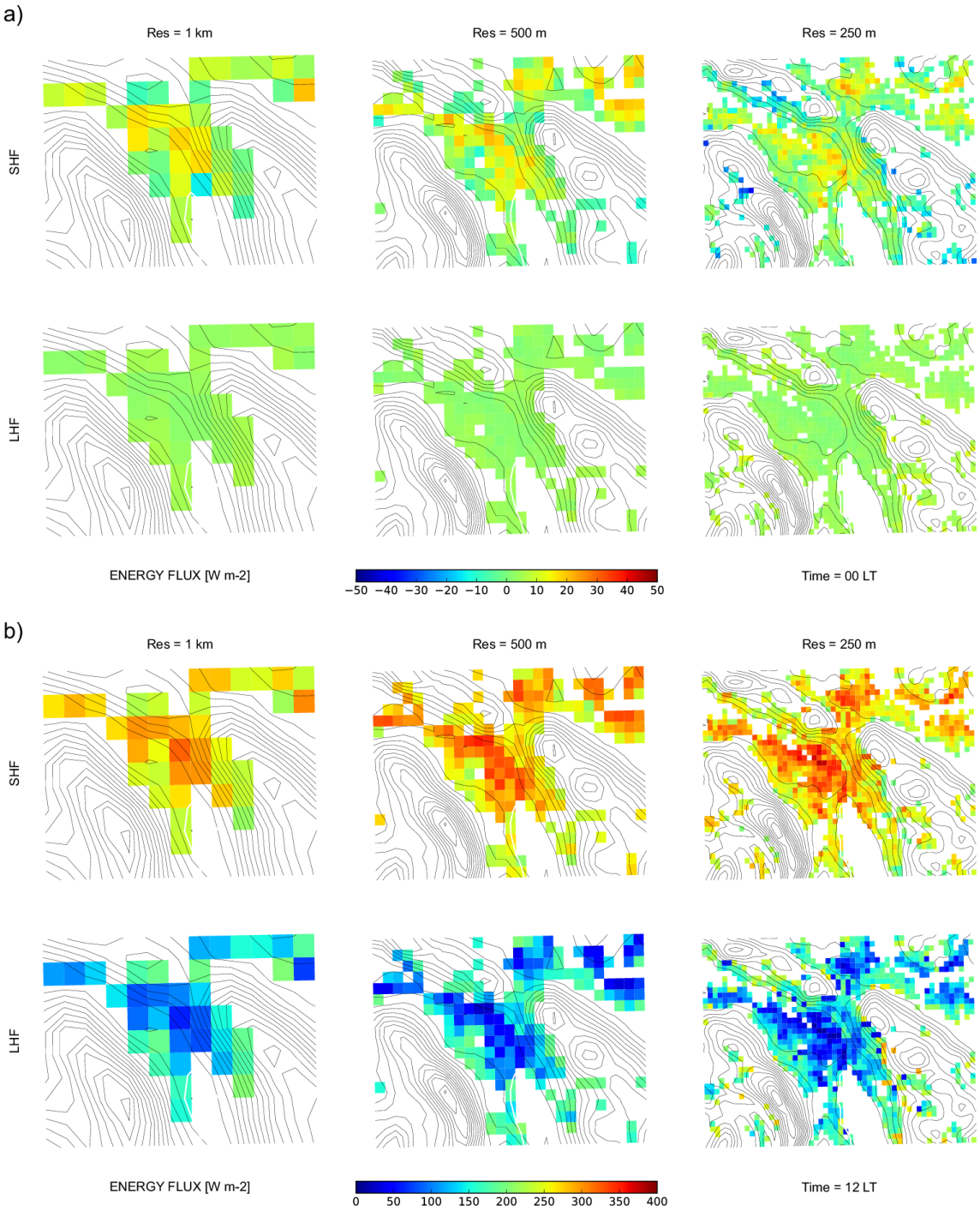


Figure 8 - Spatial distribution of the period-averaged upward surface sensible heat flux (SHF) and latent heat flux (LHF) at 00 LT and 12 LT for CCLM-DCEP at the different grid spacings in the urban area. Only urban grid cells are shown.

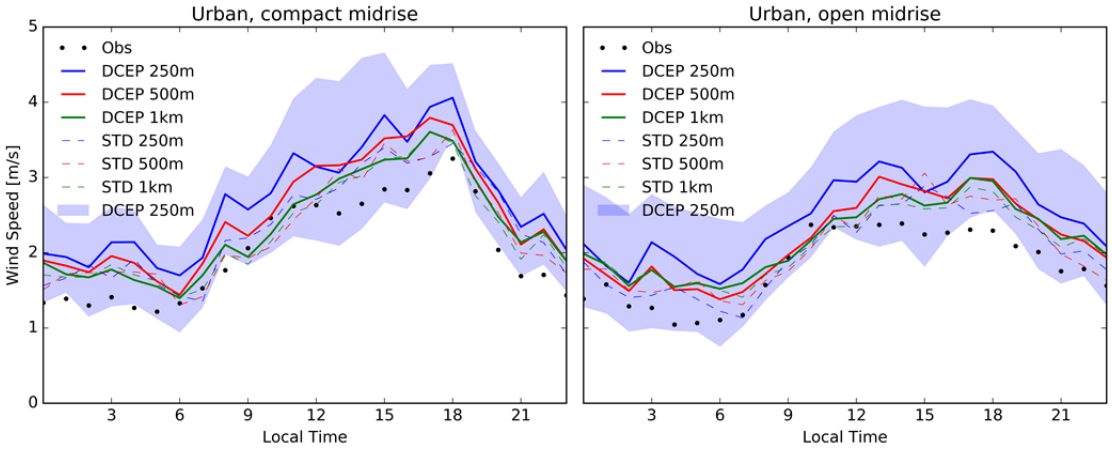


744

745 Figure 9 - Observed and simulated period-averaged diurnal cycle of wind speed at different hor-
746 izontal grid spacing at compact urban and open urban sites. The solid and dotted lines indicate
747 the simulation with CCLM-DCEP and CCLM-STD, respectively.

748

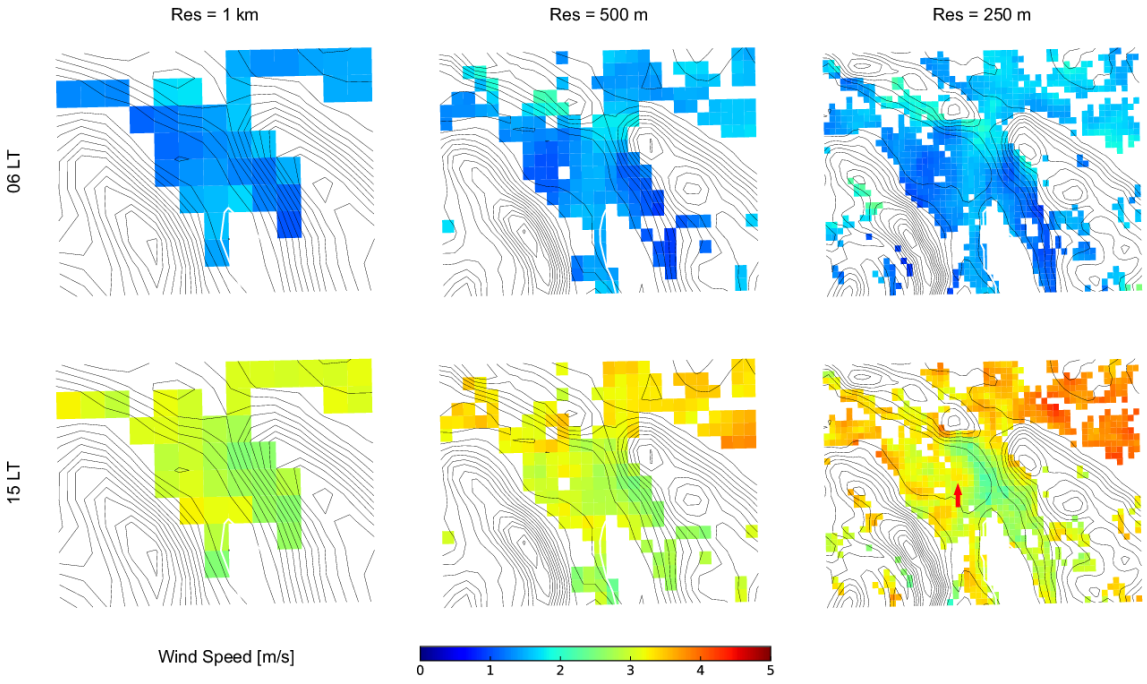


749

750 Figure 10 - Simulated period-averaged spatial distribution of 10-m wind speed [m s-1] at 06 LT
751 and 15 LT using CCLM-DCEP with model grid spacing of 1 km, 500m and 250m, respectively.
752 The red arrow indicates the location of the railway.

753